



# Effects of Arctic sea ice in autumn on extreme cold events over the Tibetan Plateau in the following winter: possible mechanisms

Miao Bi<sup>1,2</sup> · Qingquan Li<sup>1,2</sup> · Song Yang<sup>3,4</sup> · Dong Guo<sup>1</sup> · Xinyong Shen<sup>1,4</sup> · Xiaoting Sun<sup>1,2</sup>

Received: 28 April 2021 / Accepted: 11 October 2021 / Published online: 30 October 2021  
© The Author(s) 2021

## Abstract

Extreme cold events (ECEs) on the Tibetan Plateau (TP) exert serious impacts on agriculture and animal husbandry and are important drivers of ecological and environmental changes. We investigate the temporal and spatial characteristics of the ECEs on the TP and the possible effects of Arctic sea ice. The daily observed minimum air temperature at 73 meteorological stations on the TP during 1980–2018 and the BCC\_AGCM3\_MR model are used. Our results show that the main mode of winter ECEs over the TP exhibits the same spatial variation and interannual variability across the whole region and is affected by two wave trains originating from the Arctic. The southern wave train is controlled by the sea ice in the Beaufort Sea. It initiates in the Norwegian Sea, and then passes through the North Atlantic Ocean, the Arabian Sea, and the Bay of Bengal along the subtropical westerly jet stream. It enters the TP from the south and brings warm, humid air from the oceans. By contrast, the northern wave train is controlled by the sea ice in the Laptev Sea. It originates from the Barents and Kara seas, passes through Lake Baikal, and enters the TP from the north, bringing dry and cold air. A decrease in the sea ice in the Beaufort Sea causes positive potential height anomalies in the Arctic. This change enhances the pressure gradient between the Arctic and the mid-latitudes, leading to westerly winds in the northern TP, which block the intrusion of cold air into the south. By contrast, a decrease in the sea ice in the Laptev Sea causes negative potential height anomalies in the Arctic. This change reduces the pressure gradient between the Arctic and the mid-latitudes, leading to easterly winds to the north of the TP, which favors the southward intrusion of cold polar air. A continuous decrease in the amount of sea ice in the Beaufort Sea would reduce the frequency of ECEs over the TP and further aggravate TP warming in winter.

**Keywords** Arctic sea ice · Tibetan Plateau · Extreme cold event · Rossby wave activity

## 1 Introduction

Sea ice in the Arctic region has been melting at an unprecedented rate and record low coverage has been repeatedly observed. According to the latest data from the US National Snow and Ice Data Center, the area of sea ice in October 2020 was 5.28 million square kilometers, the lowest since satellite records began. This was 450,000 square kilometers less than the previous lowest October record set in 2019. The Arctic climate system has undergone dramatic changes since the start of the twenty-first century (Wu 2018; Ma and Zhu 2019; Ding 2021). The accelerated melting of sea ice and the rapid evolution of Arctic vegetation and ecosystems have led to further physical and biochemical changes in the oceans (Koenigk et al. 2020). More heat is transferred from the oceans to the atmosphere at the high latitudes. Temperature gradients at the middle-high latitudes of the northern hemisphere are therefore weakened, leading to a weakening of the

✉ Qingquan Li  
liqq@cma.gov.cn

✉ Dong Guo  
dongguo@nuist.edu.cn

<sup>1</sup> Collaborative Innovation Center on Forecast and Evaluation of Meteorological Disasters/Key Laboratory of Meteorological Disaster, Ministry of Education/Joint International Research Laboratory on Climate and Environment Change, Nanjing University of Information Science and Technology, Nanjing 210044, China

<sup>2</sup> Laboratory for Climate Studies, National Climate Center, China Meteorological Administration, Beijing 100081, China

<sup>3</sup> School of Atmospheric Sciences and Guangdong Province Key Laboratory for Climate Change and Natural Disaster Studies, Sun Yat-Sen University, Zhuhai 519082, China

<sup>4</sup> Southern Marine Science and Engineering Guangdong Laboratory (Zhuhai), Zhuhai 519082, China

westerly wind belt and baroclinicity in these regions (Zhu et al. 1999; Outten and Esau 2012; Overland et al. 2012; Zhao et al. 2015; Wu et al. 2019a). The baroclinic instability of baroclinic and planetary waves begins earlier (Bader et al. 2011) and the intensities of polar low pressure regions and polar front jet streams are also affected (Zahn and Storch 2010). The number of extreme cold waves in Europe, East Asia and North America has increased (Kim et al. 2014; Gao et al. 2015; Wu et al. 2017; Ma and Zhu 2020).

The decrease of SIC in early autumn is closely related to the tripolar pattern of surface winds in the middle-high latitudes of Eurasia in winter and is negatively related to the intensity of the Siberian high (Hu et al. 2004; Wu et al. 2011; Chen and Wu 2014; Chen et al. 2020). The SIC on the eastern side of Greenland decreases and a negative phase of the Arctic Oscillation or North Atlantic Oscillation appears, which facilitates an intrusion of cold air from the Arctic to Europe, leading to widespread cooling (Alexander et al. 2004; Hu and Wu 2004; Hu and Huang 2006; Li et al. 2005; Wu et al. 2018). Li et al. (2021) found that changes in the amount of sea ice in the Barents Sea in March affected the circulation and temperature anomalies in eastern China through the Silk Road teleconnection, leading to a “warm in the south and cold in the north” mode of surface temperatures in eastern China in August. Variations in the Arctic SIC and the corresponding atmospheric circulation are therefore important reasons for the decreasing trend in surface temperatures and the frequent occurrence of ECEs over the Eurasian continent in winter (Wu et al. 1999, 2013, 2015; Honda et al. 2009; Hopsch et al. 2012; Jaiser et al. 2012; Peings et al. 2014).

The vast and complex terrain of the Tibetan Plateau (TP), often referred to as the “Roof of the World” or the “Third Pole”, serves as a diver and an amplifier of global climate change (Chen and Wu 2000; Lu et al. 2011; Liu et al. 2014). The TP often experiences extreme weather and climate events and, like the Arctic SIC, is indicative of global climate change. Cold events in winter over the TP most apparently occurred in the 1960s and 1980s, while warm events mainly appear in the 1990s and early twenty-first century (Wu et al. 2005; Zhou et al. 2019; Suolang et al. 2020).

Among the limited studies on the impact of Arctic sea ice on the TP, Jiao et al. (2017) analyzed the characteristics of the ECEs in autumn and winter over the TP from 1979 to 2011 and found a decreasing trend. The ECEs over the TP are significantly negatively correlated with the SIC in the key areas of the Laptev Sea–eastern Siberian Sea and the Beaufort Sea–Baffin Bay regions. The lack of sea ice in these key areas leads to a negative–positive–negative (– + –) pattern in the 500 hPa geopotential height of the polar and plateau regions and a Rossby wave from north to south over the TP. Gu et al. (2018) analyzed the relationship between the Arctic SIC and the weather at

mid-latitudes and found that the transient vortices over the TP are closely related to the SIC. The activity of transient vortices, the meridional circulation, the westerly jet stream and the high-altitude trough and ridge pattern are all inter-restricted internal units and correspond to dramatic changes in temperature over the TP (also see Ren et al. 2021). Zhang et al. (2019) analyzed the winter snow anomalies on the TP and showed that the wave activity from the Arctic could reach the TP through both northern and southern routes when the atmospheric circulation is in a coupled mode of the positive phase of the Arctic Oscillation (+ AO) and the negative phase of the Western Pacific (– WP) teleconnection. This creates the dynamic and moisture conditions required for snowfall over the TP and therefore connects the TP with the Arctic. No wave activity could reach the TP when only one of these conditions was present.

Moreover, Li et al. (2020) analyzed the influence of the winter SIC in the North Atlantic on the transport of aerosols from the TP. The polar front jet is weakened when the North Atlantic subpolar SIC decreases, which reduces the amount of warm and humid oceanic air entering the northern Eurasian continent, further reducing snow cover in the Ural Mountains. This strengthens both the high-pressure ridge in the Ural Mountains and the East Asian trough, forming a quasi-stationary Rossby wave across the Eurasian continent. These conditions lead to an increase in the subtropical westerly jet stream at the southern edge of the TP and an increase in the combination of upslope winds and mesoscale updrafts, which favors a discharge of pollutants over the Himalaya. Yang et al. (2020) used reanalysis datasets to depict the characteristics of ECEs in the northern hemisphere in winter and their relationships with the Arctic SIC in autumn. The ECEs in the northern hemisphere showed north–south reverse-phase changes and the TP was located at the center of a high-temperature anomaly that was significantly and positively correlated with the SIC in the Beaufort Sea and the Barents Sea–Kara Sea in autumn. The ECEs on the TP exert serious impacts on agriculture and animal husbandry and are important drivers of ecological and environmental changes. However, there have been relatively few studies on the relationship between the extreme climate change over the TP and the Arctic SIC, and thus the responsible mechanisms can hardly be understood. In this paper, we intend to investigate these issues to understand the mechanism for the ECE variations over the TP, which will be helpful for predicting extreme events and providing a scientific basis for disaster prevention and mitigation.

The organization of the paper is as follows. Data and methods are described in Sect. 2. The main results obtained are shown in Sect. 3. Section 4 presents the summary and discussions.

## 2 Data and methods

We use the relatively complete dataset of the daily observed minimum air temperature from 73 meteorological stations on the TP (Duan 2008). These data are based on the six-hourly observed air temperature from > 2400 meteorological stations in China for 1980–2018 provided by the National Meteorological Information Center of the China Meteorological Administration. Since the stations are mainly distributed in the eastern TP region, with only several stations in the western TP, we also analyze the temperature climate index from the HadEX3 data with a horizontal resolution of  $1.25^\circ \times 1.875^\circ$  (Dunn et al. 2020) to confirm the reliability of the results obtained.

Moreover, we use the ERA5 reanalysis dataset (Hersbach et al. 2020) from 1980 to 2018 provided by the European Centre for Medium-range Weather Forecasts (ECMWF). The variable elements include the vertical 37-layer geopotential height, zonal and meridional wind, the surface pressure and the 2-m air temperature at a horizontal resolution of  $0.25^\circ \times 0.25^\circ$ . Monthly SIC data with a horizontal resolution of  $1^\circ \times 1^\circ$  from 1980 to 2018 provided by the UK Hadley Center (Rayner et al. 2003) is also applied.

A number of statistical and diagnostic methods such as the Empirical Orthogonal Function (EOF), detrending, correlation, composite, linear regression analysis and Student's *t* test have been employed in this study. Autumn is defined as September–October–November, and winter from December to February of the following year. The definition of the Expert Team on Climate Change Detection and Indices (Karl et al. 1999; Peterson 2005) is used to calculate the number of days with ECEs based on the daily observed minimum temperature. The daily minimum temperature data of 73 stations in winter from 1980 to 2018 are arranged in ascending order, and the value of 10th percentile is defined as the ECE threshold of the stations. If the minimum temperature of the station on a certain day is lower than the threshold, it is considered occurrence of an ECE at the station on that day. The total number of days with an ECE at a single station in the TP from 1980 to 2018 is calculated statistically (TN10p) when the daily minimum temperature is < 10% threshold. To eliminate the influence of synoptic-scale disturbances, a seven-point moving average is applied before the statistical threshold (Ren et al. 2017). We remove all variables from the long-term linear trends before synthesis and correlation analysis. The three-dimensional wave flux under quasi-geostrophic conditions defined by Takaya and Nakamura (2001) is used to determine the fluctuations related to the air temperature over the TP and the Arctic SIC as follows:

$$W = \frac{1}{2|U|} \left\{ \begin{array}{l} \bar{u}(\varphi_x'^2 - \varphi' \varphi_{xx}') + \bar{v}(\varphi_x' \varphi_y' - \varphi' \varphi_{xy}') \\ \bar{u}(\varphi_x' \varphi_y' - \varphi' \varphi_{xy}') + \bar{v}(\varphi_y'^2 - \varphi' \varphi_{yy}') \\ \frac{f^2}{R\sigma p^{-1}} \left\{ \bar{u}(\varphi_x' \varphi_p' - \varphi' \varphi_{xp}') + \bar{v}(\varphi_y' \varphi_p' - \varphi' \varphi_{yp}') \right\} \end{array} \right\} \quad (1)$$

$$\sigma = \frac{R\bar{T}}{C_p p} - \frac{d\bar{T}}{dp} \quad (2)$$

where  $\varphi'$  denotes the disturbed stream function,  $f$  is the Coriolis parameter,  $R$  is the gas constant,  $|U| = (u, v)$  is the horizontal wind velocity,  $T$  is the temperature,  $p$  is the pressure and  $C_p$  is the specific heat at constant pressure.

To better understand the observational results, we utilize the Beijing Climate Center Atmosphere General Circulation model (BCC\_AGCM3\_MR) to conduct a series of numerical experiments. The model has a horizontal resolution of  $1.875^\circ \times 1.875^\circ$ , and 46 vertical levels. It is developed by National Climate Center of China Meteorological Administration on the basis of the Community Atmosphere Model version 3 (CAM3) of the US National Center for Atmospheric Research (NCAR), and has been widely applied in climate researches (Wu et al. 2019b). The integration duration of all experiments is 55 years. In order to avoid the deviation caused by the instability of the initial of the model, the data of the first 20 years are discarded and the results of the last 35 years are analyzed.

## 3 Results

### 3.1 Temporal and spatial characteristics of ECEs over the Tibetan Plateau

We perform an EOF analysis on the anomalous days of ECEs over the TP in winter. Figure 1 shows the first EOF mode, which explains 37.71% of the total variance. The ECEs over the TP show a uniform mode throughout the region, although the variability in the northern TP is slightly greater than that in the south (Fig. 1a). The time coefficient shows clear interannual variations. ECEs were more frequent in the 1990s and less frequent in the early twenty-first century (Fig. 1c). Overall the first EOF mode shows a decreasing but insignificant trend, consistent with the result from previous results (Jiao et al., 2017). Figure 1b shows the result of the HadEX3 data, which also exhibits a uniform EOF1 mode as in station observations. The correlation coefficient between the EOF1 time series of the two datasets is 0.72 (passing the significance test of 99% confidence level). Considering that the HadEX3 data interpolated from 316 stations in China only include 35 stations in the eastern TP, we adopt the observation dataset from 73 stations in the following

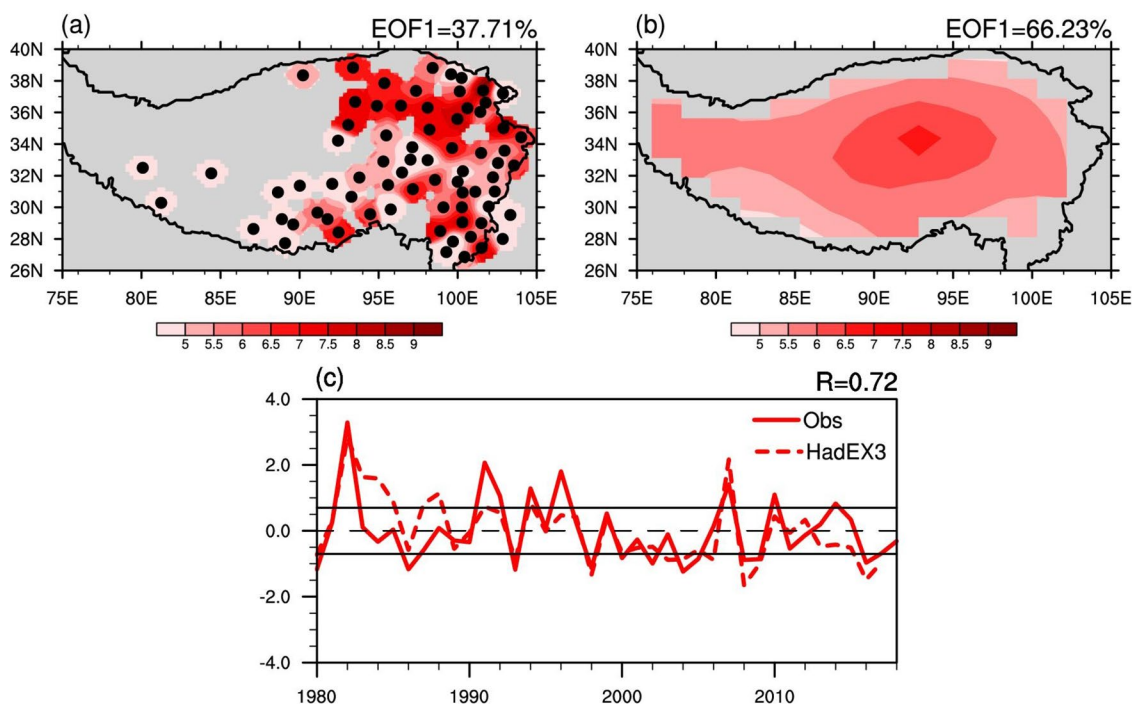


**Fig. 1** The first EOF (EOF1) mode of the winter ECEs (shading; day) of **a** observations of 73 meteorological stations and **b** HadEX3 data over the TP during 1980–2018. **c** Standardized EOF1 time coefficients of the winter ECEs of the observational stations (red solid

curve) and HadEX3 data (red dashed curve). The black dots in Fig. 1a indicate the locations of the observational stations, and black solid lines in Fig. 1c represent 0.7 standard deviations

analysis. We define the standardized time coefficient of the first EOF mode as the TN10p index of the TP.

### 3.2 Atmospheric circulation associated with ECEs over the Tibetan Plateau in winter

According to the standardized TN10p index (Fig. 1c), eight high-TN10p index years (1982, 1991, 1992, 1994, 1996, 2007, 2010 and 2014) with standard deviations  $> 0.7$  were selected to represent the years with frequent occurrences of ECEs over the TP. Eleven years of low-TN10p index (1980, 1986, 1993, 1998, 2000, 2002, 2004, 2005, 2008, 2009 and 2016) with standard deviations less than  $-0.7$  were selected to represent the years with a rare occurrence of ECEs. The possible causes of the ECEs were explored through composite analyses of the atmospheric circulation.

We calculated the difference in the atmospheric circulation in winter between the years of low- and high-TN10p indices (Fig. 2). The geopotential height anomaly exhibits an equivalent barotropic structure at 250 hPa and 500 hPa. The Arctic region is generally controlled by positive geopotential height anomalies. There was a “+ - + - +” wave train along the subtropical westerly jet stream from the North Atlantic–western Europe to Saudi Arabia–northern Indian Ocean–TP. There was also a negative height anomaly over Lake Baikal, indicating the trough deepening in this area.

The distribution of the difference in wave activity flux between the years of low- and high-TN10p indices shows two branches of wave activity flux propagating from the Arctic. The southern branch of the wave train (SBWT) originates from the Arctic Ocean and the Norwegian Sea. It travels southeastwards through the North Atlantic and Eurasia along the subtropical westerly jet stream and passes through the Arabian Sea and the Bay of Bengal before reaching the southern TP. This branch brings warm, humid air from the ocean to the TP. The correlation coefficient between the TN10p index and the subtropical westerly jet stream index was 0.5, significantly passing 99% confidence level (figure not shown). Therefore, we refer to this branch as the wave train captured by the subtropical westerly jet stream. Li et al. (2020) analyzed the mechanism for the influence of Arctic sea ice on aerosol emissions from the TP, and explained the role of the subtropical westerly jet stream in this bridge between the TP and the Arctic.

By contrast, the northern branch of the wave train (NBWT) originates from the Barents Sea–Kara Sea, extends to the north of China, passes through Lake Baikal and reaches the northern TP. This feature favors the invasion of cold air from the north. We calculated the difference in the vertical wave activity flux between the low- and high-TN10p index years and found that the two wave trains from the North Pole were related to the variations in the SIC. Figure 3

**Fig. 2** Composite differences in **a** 250 hPa and **b** 500 hPa geopotential heights (shading; gpm) and wave activity fluxes (vectors;  $m^2/s^2$ ) in winter between low- and high-TN10p index years. The thick red and blue contours denote wind speeds of 40 and 20 m/s, respectively. The light and dark purple dots indicate the geopotential height differences significantly exceeding 90% and 95% confidence levels, respectively

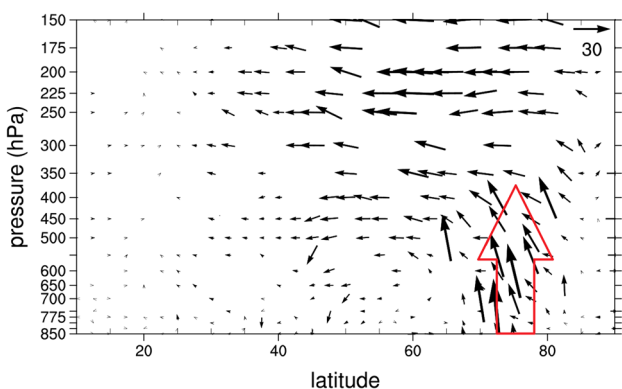
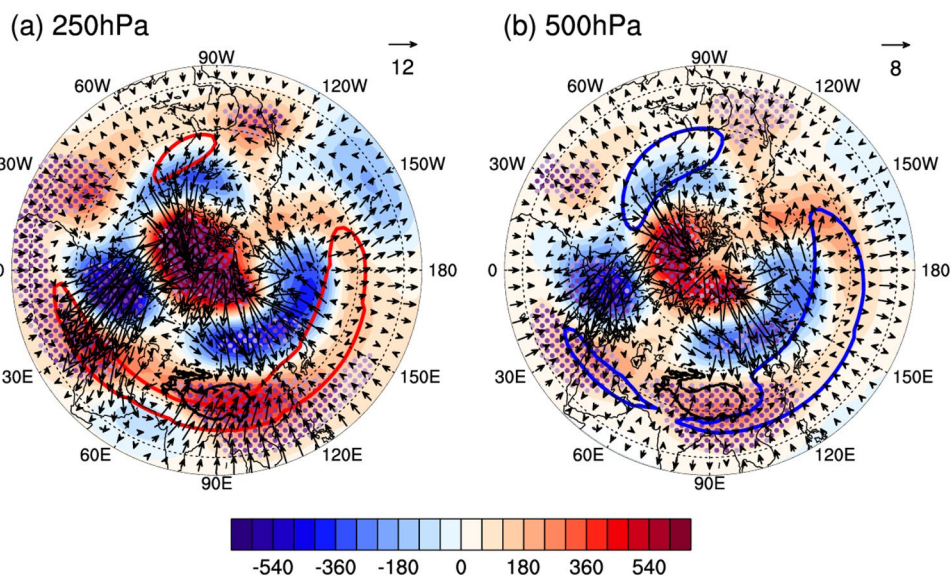


**Fig. 3** Composite differences in the vertical component of wave activity flux (vectors;  $Pa \cdot m/s^2$ ) in winter between low- and high-TN10p index years

shows the distribution of the wave activity flux with altitude along  $0^\circ$  longitude, the origin longitude of the two wave trains. Anomalous wave activity flux propagates upward and to the middle-low latitudes from the Arctic region. When sea ice changes, the temperature gradient in the edge region will change, which further results in the baroclinity of the changed lower atmosphere, triggers the planetary wave-number 1 and wave-number 2, and affects the atmospheric heat flux (Zahn et al. 2010; Inoue et al. 2012). We therefore conclude that the number of days with ECEs over the TP is related to the anomalies of the Arctic SIC.

### 3.3 Association of the SIC in key Arctic areas with winter ECEs over the Tibetan Plateau

Our results indicate that the variation of the ECEs over the TP is closely related to the Arctic SIC. We therefore

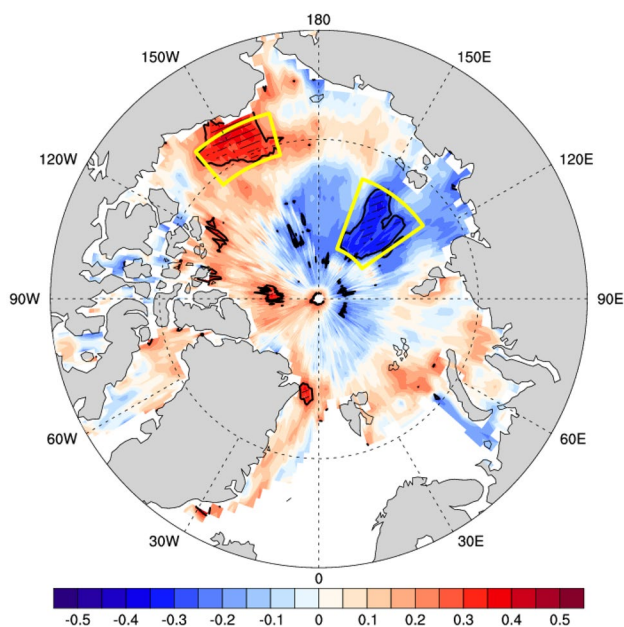


**Fig. 4** Correlation coefficients between the TN10p index in winter and the Arctic SIC in autumn. The 90% and 95% confidence levels are denoted by black thick contour and cross hatching, respectively

calculate the correlation of the TN10p index with the Arctic SIC in autumn after removing the long-term linear trend of the SIC and the TN10p index. Figure 4 shows that there are two regions in the Arctic where the TN10p index is significantly correlated with the Arctic SIC in autumn: the Arctic Ocean portion close to the northern Laptev Sea ( $120\text{--}160^\circ E, 75\text{--}85^\circ N$ ) and the Beaufort Sea ( $165\text{--}140^\circ W, 72\text{--}76^\circ N$ ). These areas are referred to as the key areas of SIC. The autumn SIC in the Laptev Sea–East Siberian Sea is negatively correlated with the winter TN10p index

of the TP, whereas the SIC in the Beaufort Sea is positively correlated with the winter TN10p index of the TP. Therefore the effects of the SIC in autumn on the ECEs in winter are the opposite in these two key areas. The number of days of ECEs over the TP decreases when the SIC in the Beaufort Sea is reduced, whereas the number of days of ECEs over the TP increases as the SIC in the Laptev Sea is reduced. This result is different from that of Jiao et al. (2017), whose analysis showed that there was a significant negative correlation between the Arctic SIC and the ECEs. A reduction in SIC would increase the number of ECEs over the TP, but could not explain the decrease in the number of ECEs.

To verify the relationship between the SIC in the key areas and the number of ECEs over the TP, we established two sea ice concentrate indexes (SICIs), the detrended standardized average SIC of the two key areas (Fig. 5). The correlation coefficient is  $-0.35$  between the Laptev Sea SICI (LSICI) and the TN10p index, and  $0.39$  between the Beaufort Sea SICI (BSICI) and the TN10p index, both significantly passing 95% confidence level. No significant correlation can be found between the BSICI and the LSICI (correlation coefficient  $-0.03$ ). This feature indicates that the SIC in the two sea areas are independent from each other.

We therefore infer that the SIC in the two key areas affects the ECEs over the TP through different mechanisms. Based on a standard deviation of 0.7, we define the years with an SICI  $> 0.7$  as heavy-ice years and the years with an SICI  $< -0.7$  as light-ice years. In the Laptev Sea, the heavy-ice years include 1996, 2001, 2002, 2004, 2013, 2016 and 2017 and the light-ice years are 2005, 2007, 2012, 2014 and 2018. In the Beaufort Sea, the heavy-ice years include 1991, 1992, 1994, 1995, 1996, 2001, 2005, 2013, 2014 and 2015 and the light-ice years are 1993,

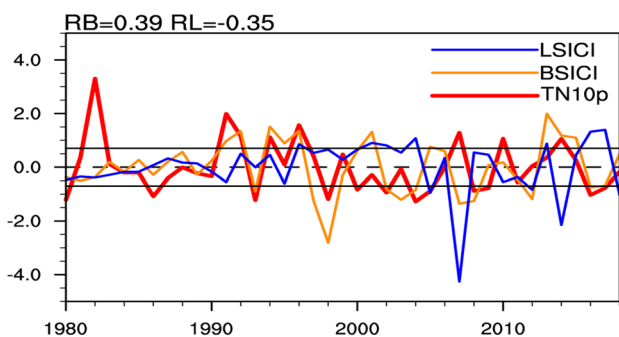


**Fig. 5** Time series of the standardized regional average SIC in the key Arctic regions in autumn. The red curve indicates the TN10p index. The orange and blue curves indicate the SIC indexes in the Beaufort Sea and the Laptev Sea in autumn, respectively. The black solid lines represent 0.7 standard deviations

1997, 1998, 2002, 2003, 2004, 2007, 2008, 2012, and 2016.

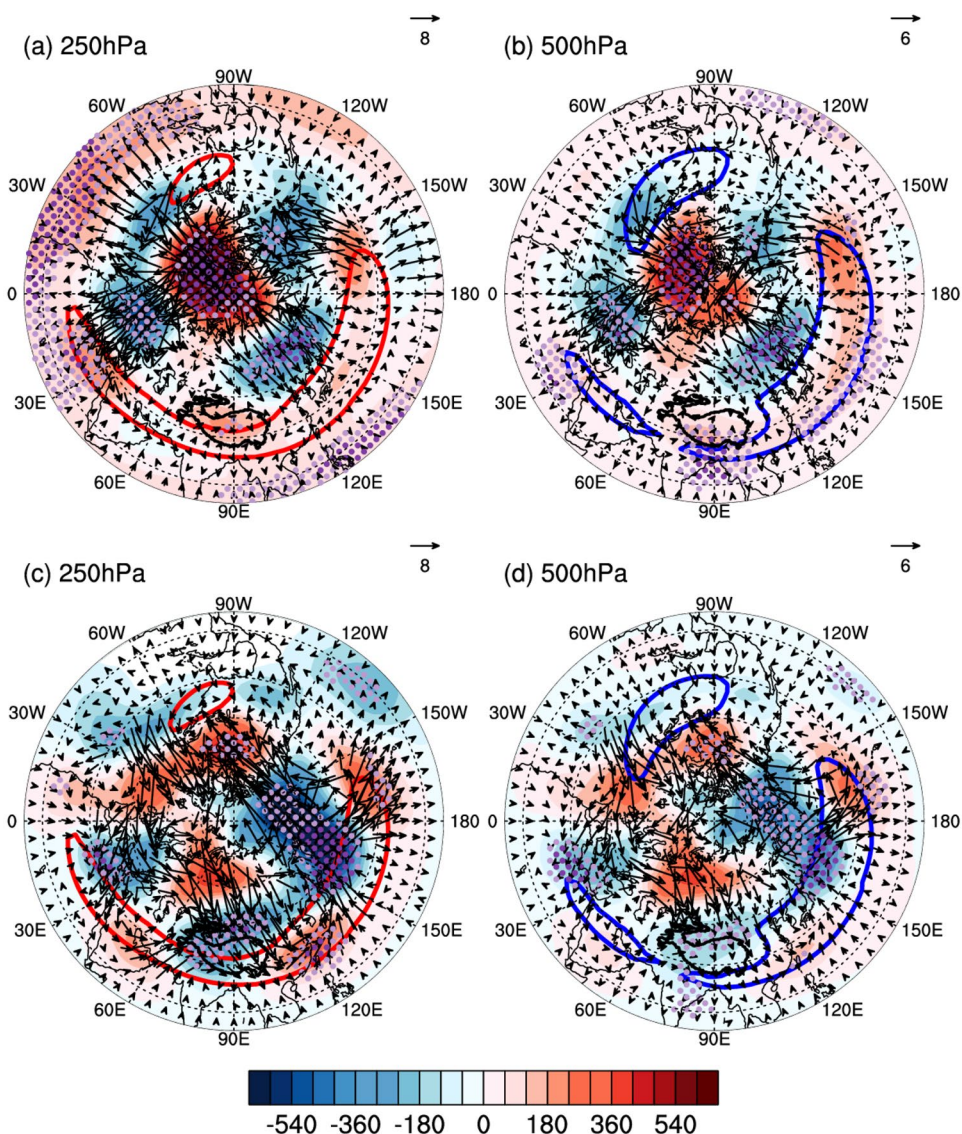
### 3.4 Regulation of the atmospheric circulation in the northern hemisphere by SIC in the key Arctic regions

We carry out a composite analysis of the heavy-ice and light-ice years based on the SIC anomalies. Figures 6a, b show that a decrease in the SIC in the Beaufort Sea results in positive geopotential height anomalies over the whole Arctic, which favors the accumulation of cold air in the Arctic, but not an intrusion of cold air into the middle-low latitudes. Western Europe–Saudi Arabia–northern Indian Ocean–TP show a “ $- + - +$ ” zonal wave train (Fig. 6a, b). When the cold air mass passes through the North Atlantic and the Indian Ocean, the subtropical jet stream acts as a waveguide (correlation coefficient between the BSICI and the subtropical westerly jet stream index is 0.32, passing the significance test of 95% confidence level). It transports warm, humid air to the TP, and thus ECEs are less likely to form. By contrast, negative anomalies in the SIC in the Laptev Sea lead to a zonal belt of positive geopotential height anomalies in northern Eurasia. This reduces the pressure gradient between the Arctic and the middle-low latitudes, and the polar cold air mass is more likely to spread southward. A decrease in the SIC in the Laptev Sea causes wave activity fluxes through northern Eurasia–Lake Baikal, transporting cold air masses from the Arctic to the TP (Fig. 6c, d). The wave activity fluxes caused by the changes in SIC in these two key areas correspond to the wave activity flux propagation pathways analyzed in Sect. 3.2.

Figure 7 shows the difference in 500 hPa wind (vectors; m/s) and the 2 m temperature (shading; K) between light-ice and heavy-ice years. A reduction in the Beaufort Sea SIC produces a significant westerly anomaly in the northern TP, which does not favor the southward movement of cold air over the TP. By contrast, a decrease in the Laptev Sea SIC forms anomalous easterly wind from Lake Baikal to the northwestern TP, strengthening meridional activity. The decrease in the Beaufort Sea SIC leads to a decrease in temperature in northern Eurasia and an increase in temperature in southern Eurasia, which increases the difference in temperature between the north and the south, and the TP becomes warmer. By contrast, a reduction in the Laptev Sea SIC reduces the north–south temperature gradient, favoring the southward movement of cold air.

The surface pressure in the entire polar region increases when the SIC in the Beaufort Sea decreases (Fig. 8a), which does not favor the southward movement of cold air. The TP presents a significant positive surface pressure anomaly (Fig. 8a) and therefore the warm air from the Indian Ocean accumulates over the TP. By contrast, when the SIC in the

**Fig. 6** Composite differences in **a** 250 hPa and **b** 500 hPa geopotential heights (shading; gpm) and wave activity fluxes (vectors;  $m^2/s^2$ ) in winter between light-ice years and heavy-ice years in the Beaufort Sea. Composite differences in **c** 250 hPa and **d** 500 hPa geopotential heights (shading; gpm) and wave activity fluxes (vectors;  $m^2/s^2$ ) in winter between light-ice and heavy-ice years in the Laptev Sea. The thick red and blue contours denote wind speeds of 40 and 20  $m/s$ , respectively. The light and dark purple dots indicate geopotential height differences significantly exceeding 90% and 95% confidence levels, respectively



Laptev Sea decreases, there is a negative surface pressure in the Arctic and a positive surface pressure at middle-low latitudes (Fig. 8b). This favors the extension of cold air southward, forming ECEs over the TP. However, most of the correlation is insignificant, which may indicate that the SIC in the Laptev Sea exerts little effect on the TP.

The effects of autumn SIC on winter TP ECEs is opposite between the two key areas. To determine the relative effects of the SBWT and the NBWT on the ECEs, we use binary linear regression to calculate the partial correlation coefficients between the SIC in the two key areas and the number of days with ECEs at each station on the TP. The two-dimensional scatter point distribution in Fig. 9a shows that there are different effects of the SIC in the two regions on the number of days with ECEs at the 73 stations on the TP. The BSICI (LSICI) is positively (negatively) correlated with the number of ECEs. The dots above the black diagonal line

(upper right corner) of the figure indicate that the absolute value of the partial correlation coefficient between the number of ECEs and the BSIC is greater than the absolute value of the partial correlation coefficient with the LSIC. The dots below the black diagonal line shows an opposite feature. In particular, 43 points are above the diagonal line and 36% (26 stations) of them are significantly above 90% confidence level. There are a total of 30 points below the diagonal line and 30% (22 stations) of them are significant (above 90% confidence level). In general, the SIC in the Beaufort Sea (SBWT) exerts a greater impact on the TP ECEs.

Figure 9b shows the spatial distribution of the relative contributions of the SIC in different key areas to the ECEs at each station on the TP. There is a total of 43 stations in the southern TP for which the Beaufort Sea makes a large contribution to the ECEs (absolute value of the partial regression coefficient ratio > 1) at 56% (24 stations) (blue dots).

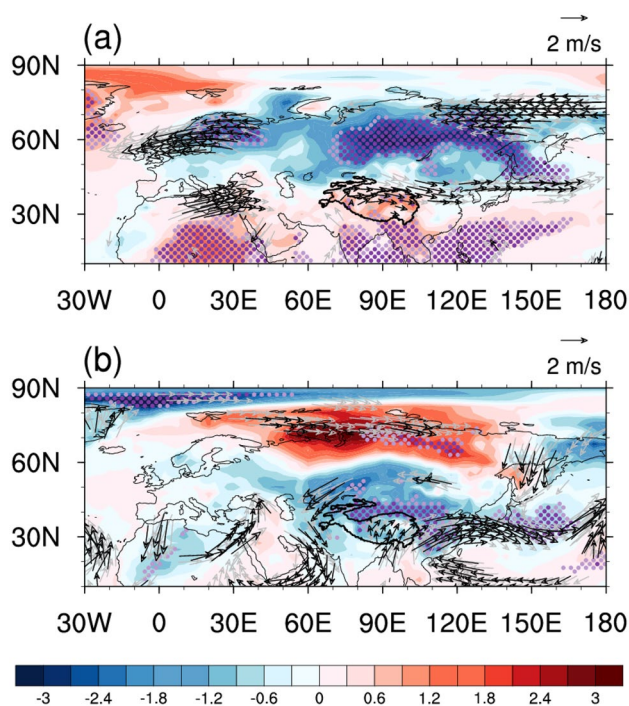


**Fig. 7** Composite differences in 500 hPa wind (vectors; m/s) and 2 m air temperature (shading; K) in winter between light-ice and heavy-ice years in **a** Beaufort Sea and **b** Laptev Sea. The black vectors pass the significance test at 95% confidence level. The light and dark purple dots indicate 2 m air temperature differences significantly exceeding 90% and 95% confidence levels, respectively

There is a total of 30 stations in the northern TP for which the Beaufort Sea makes a large contribution to the ECEs (absolute value of the partial regression coefficient ratio  $> 1$ ) at 63% (19 stations). The influence of the BSIC on the TP ECEs is therefore greater than the effect of the LSIC. That is, the influence of the SBWT on the TP is greater than influence of the NBWT.

We further perform experiments with the BCC\_AGCM3\_MR to corroborate the findings from observational analysis. Based on the observed Beaufort SIC index and Laptev SIC index, we chose the years of sea ice anomalies. We only focus on the climate anomalies caused by the anomalous SIC in the two key regions, with other external variables fixed. Five groups of experiments are conducted. The first experiment was control experiment, in which the SIC and SST adopt the climate from 1980–2010. For the second group, SIC corresponds to the climatic SIC and the Beaufort anomalous positive SIC in autumn. For the third group, SIC corresponds to the climatic SIC and the Beaufort anomalous negative SIC in autumn. For the fourth group, SIC corresponds to the climatic SIC and the

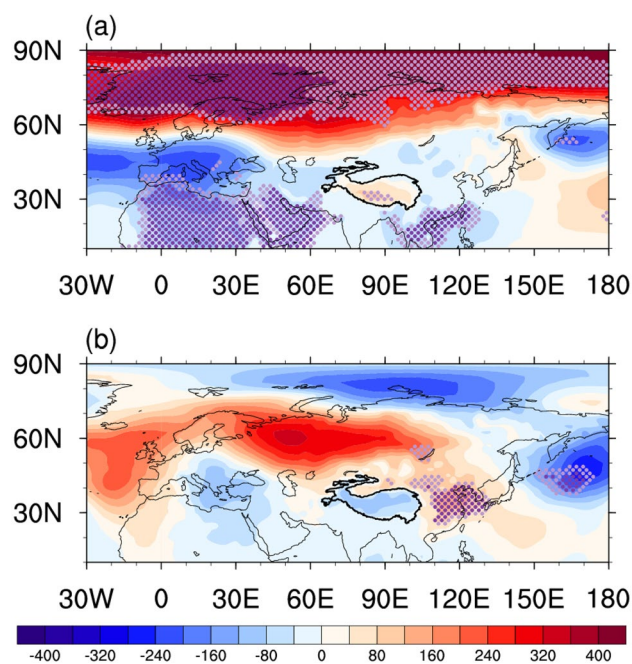


**Fig. 8** Composite difference in surface pressure (shading; Pa) in winter between light-ice and heavy-ice years in **a** Beaufort Sea and **b** Laptev Sea. The light and dark purple dots indicate the significant surface pressure differences above 90% and 95% confidence levels, respectively

Laptev anomalous positive SIC in autumn. Finally, for the fifth group, SIC corresponds to the climatic SIC and the Laptev anomalous negative SIC in autumn. The results shown hereafter mainly refer to the differences between these experiments.

Figures 10a–d represent the composite differences in the observed (Fig. 10a, b) and simulated (Fig. 10c, d) 250 hPa geopotential heights and wave activity fluxes. From the simulated results, we can still clearly find the two wave trains, the southern (Fig. 10a, c) and northern (Fig. 10b, d) trains, that affect the TP. The decrease in the Beaufort Sea ice forms a polar high pressure, while the decrease in the Laptev Sea ice is the opposite. Figures 11a–d show the composite differences in the observed (Fig. 11a, b) and simulated (Fig. 11c, d) 2 m air temperatures. It can be seen that the decrease in the sea ice in the Beaufort Sea (Fig. 11a, c) leads to a decrease in temperature in northern Eurasia and an increase in southern Eurasia, which enhances the gradient between the north and the south. This doesn't favor the southward movement of cold air over the TP, and thus the TP becomes warmer. By contrast, a reduction in the SIC in the Laptev Sea (Fig. 11b, d) reduces the north–south temperature gradient, favoring the southward movement of cold air.



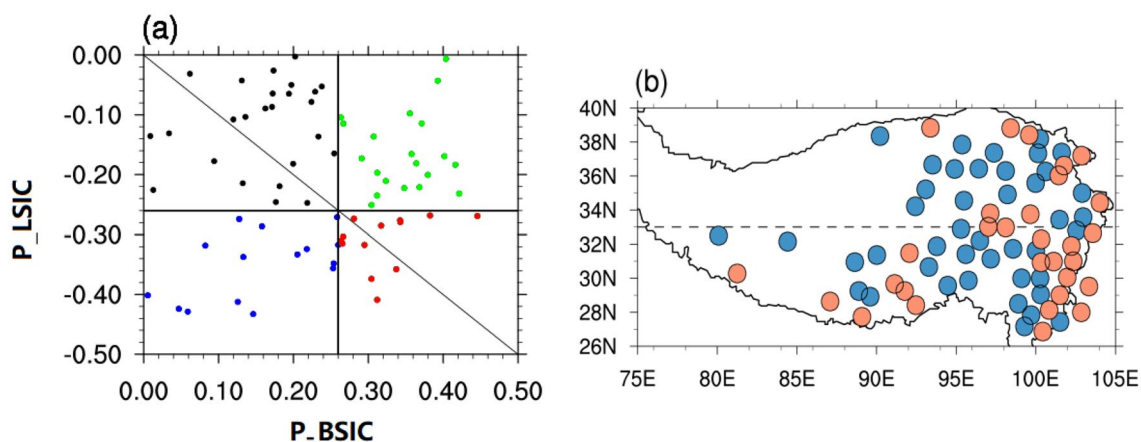
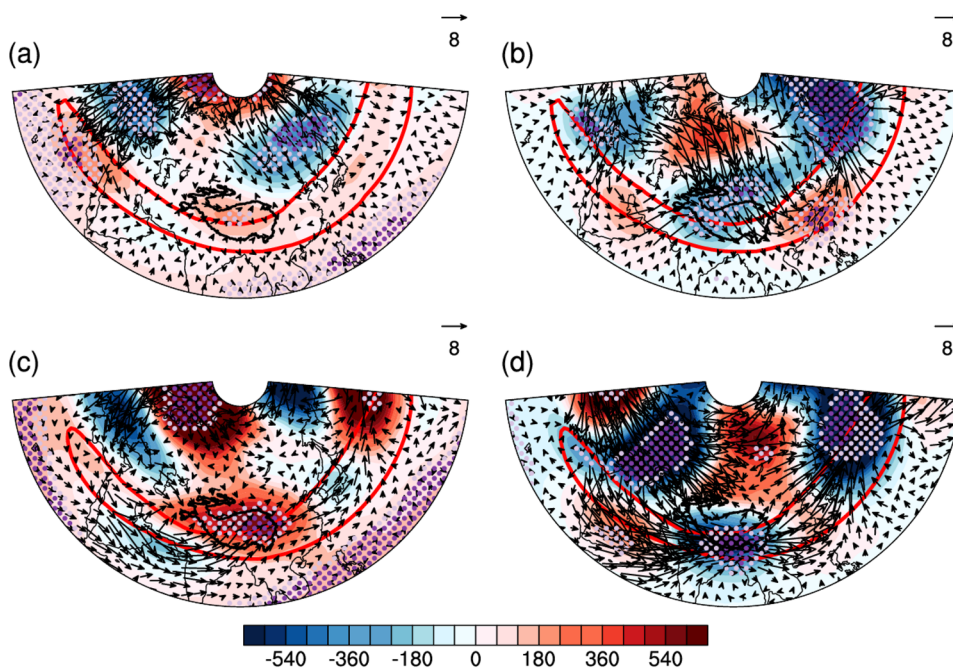


**Fig. 9** **a** Two-dimensional scatter distribution of the partial correlation coefficients between the BSICI, the LSICI and the number of days with ECEs at each station on the TP. The black dots indicate the sites where the correlation coefficients do not pass the significance test. The blue and green dots indicate the sites where the partial correlation coefficients of the LSICI and the BSICI pass the significance test at 90% confidence level, respectively. The red dots indicate the sites where the correlation coefficients of both the LSICI and the

BSICI pass the significance test at 90% confidence level. **b** Relative contribution of the Beaufort and Laptev seas to winter ECEs at each station on the TP (ratio of partial correlation coefficients). The blue dots indicate stations where the influence of the SIC in the Beaufort Sea is greater than that of the SIC in the Laptev Sea, whereas the red dots indicate the stations where the influence of the SIC in the Beaufort Sea is weaker than that of the SIC in the Laptev Sea

**Fig. 10** Composite differences in the **a, b** observed and **c, d** simulated 250 hPa geopotential heights (shading; gpm) and wave activity fluxes (vectors;  $m^2/s^2$ ) between light and heavy SIC years. **a, c** Beaufort SIC; **b, d** Laptev SIC. The red thick contours denote wind speeds of 40 m/s. The light and dark purple dots indicate the geopotential height differences exceeding 90% and 95% confidence levels, respectively

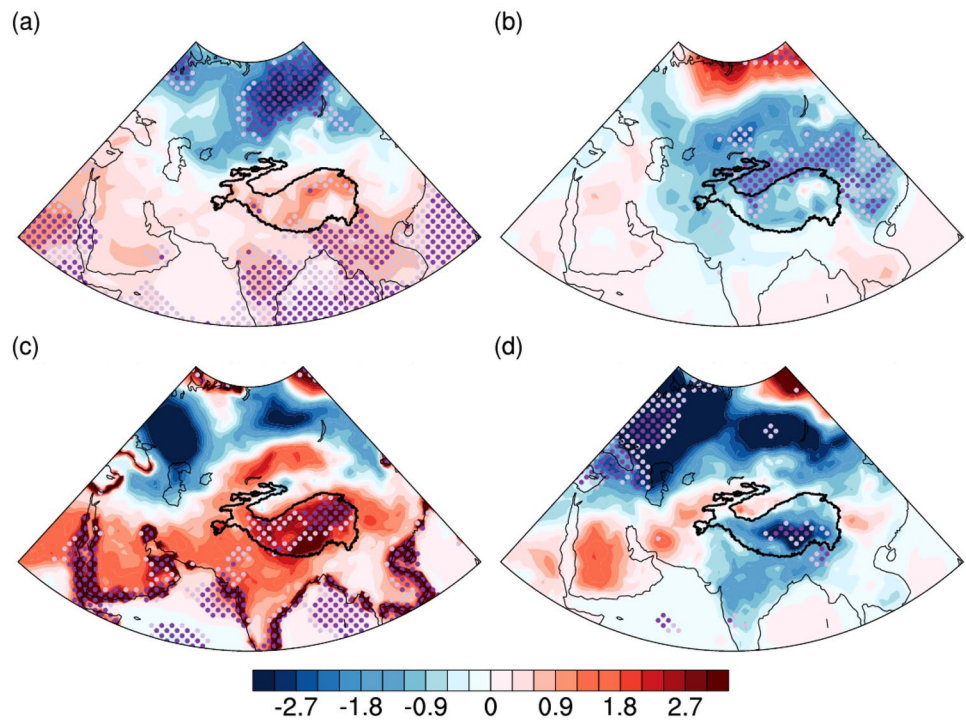


### 4 Summary and discussion

We have analyzed the possible mechanism for the impact of autumn Arctic sea ice on the ECEs in the TP. Based on analyses of both observations and model simulations, we can conclude several important features.

The main mode of the winter ECEs over the TP shows a uniform pattern over the entire region. Variability is greater in the north than in the south, with clear interannual time-scale variations. The ECEs over the TP are affected by two independent wave trains from the Arctic, the SBWT and the NBWT, and both are regulated by the SIC. The SBWT

**Fig. 11** Composite differences in the **a, b** observed and **c, d** simulated 2 m air temperatures (shading; K) between light and heavy SIC years. **a, c** Beaufort SIC; **b, d** Laptev SIC. The light and dark purple dots indicate the 2 m air temperature differences exceeding 90% and 95% confidence levels, respectively



originates in the Arctic Ocean over Iceland and the Norwegian Sea and is controlled by the Beaufort SIC. It spreads from the North Atlantic and Eurasia along the subtropical westerly jet stream to the southeast, passes through the Arabian Sea and the Bay of Bengal, and reaches the southern TP. The NBWT originates from the Barents and Kara seas, extends to the north of China, passes through Lake Baikal, and then reaches the northern TP. It is controlled by the Laptev SIC.

The processes and mechanisms through which the Arctic sea ice in autumn influences the ECEs over the TP in the following winter can be summarized in the schematic diagram presented in Fig. 12. The reduction in the Arctic SIC strengthens the meridional activity of cold air in the Arctic and the middle-high latitudes, causing a large amount of cold air to move southwards. Importantly, this explains the frequent occurrence of cold winters in the low latitudes of the northern hemisphere. Our results show

another path of the southward invasion of cold air through the North Atlantic Ocean and the North Indian Ocean, and along the subtropical westerly jet stream. The cold air mass is likely to undergo transformation when passing through warm, humid oceans and then becoming warm air mass. This provides an important explanation for the reduction in the number of ECEs over the TP. Previous studies have shown the key bridging role of the subtropical westerly jet stream in the influence of the Arctic on the TP (Wallace et al. 1988; Yang et al. 2002; Bao and You 2019; Li et al. 2020). From the observational results, the effect of the SBWT may be slightly greater than that of the NBWT, but more evidence is needed to support this feature in the future. Furthermore, the physical mechanisms responsible for the anomalies in the atmospheric circulation resulted from the variations of the SIC in key areas and the quantitative influence of the SIC on TP temperature require further investigations.

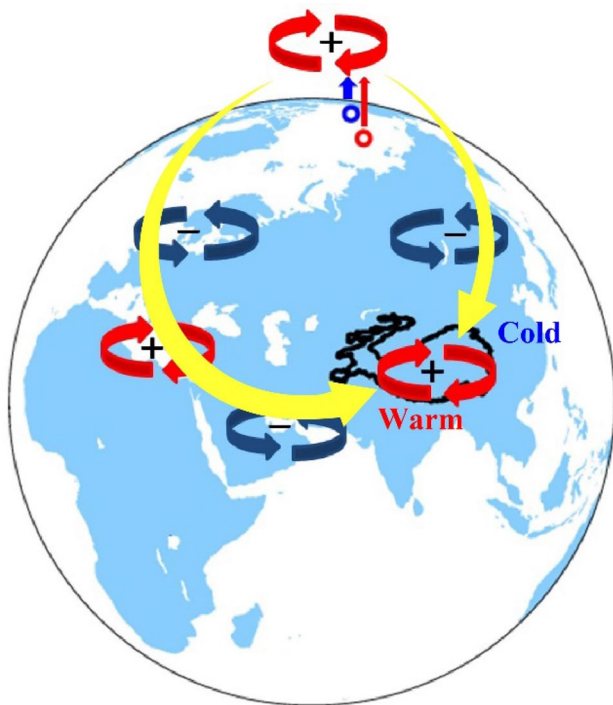


**Fig. 12** A schematic diagram illustrating the mechanism through which two key SIC regions influence the TP by two wave trains. The sea ice in two key regions weakens (strengthens) the meridional activity of Eurasia by reducing (increasing) the pressure gradient between the North Pole and mid-latitudes, forming Pole-Lake Baikal-TP wave train which brings cold air from north. Along the subtropical westerly jet stream, the North Atlantic-North Indian Ocean-TP wave train brings warm air from the oceans and exert different effects on the ECEs over the TP

**Acknowledgements** The authors are grateful to the four anonymous reviewers who have provided constructive and helpful comments on the early version of this paper. This study was jointly supported by the National Natural Science Foundation of China (41790471), the Strategic Priority Research Program of the Chinese Academy of Sciences (XDA20100304), the Second Tibetan Plateau Scientific Expedition and Research Program of China (2019QZKK0208), the National Key Research and Development Program of China (2016YFA0602200), the National Natural Science Foundation of China (41975054), Guangdong Major Project of Basic and Applied Basic Research (Grant 2020B0301030004), and Guangdong Province Key Laboratory for Climate Change and Natural Disaster Studies (Grant 2020B1212060025).

**Open Access** This article is licensed under a Creative Commons Attribution 4.0 International License, which permits use, sharing, adaptation, distribution and reproduction in any medium or format, as long as you give appropriate credit to the original author(s) and the source, provide a link to the Creative Commons licence, and indicate if changes were made. The images or other third party material in this article are included in the article's Creative Commons licence, unless indicated otherwise in a credit line to the material. If material is not included in the article's Creative Commons licence and your intended use is not permitted by statutory regulation or exceeds the permitted use, you will need to obtain permission directly from the copyright holder. To view a copy of this licence, visit <http://creativecommons.org/licenses/by/4.0/>.

## References

- Alexander MA, Bhatt US, Walsh JE et al (2004) The atmospheric response to realistic Arctic sea ice anomalies in an AGCM during winter. *J Clim* 17:890–905
- Bader J, Mesquita MD, Hodges KI et al (2011) A review on northern hemisphere sea-ice, storminess and the North Atlantic Oscillation: observations and projected changes. *Atmos Res* 101(4):809–834
- Bao YT, You QL (2019) How do westerly jet streams regulate the winter snow depth over the Tibetan Plateau? *Clim Dyn* 53:353–370
- Chen LT, Wu RG (2000) Interannual and decadal variations of snow cover over Qinghai-Xizang Plateau and their relationships to summer monsoon rainfall in China. *Adv Atmos Sci* 17:18–30
- Chen Z, Wu RG (2014) Impacts of autumn Arctic sea ice concentration changes on the East Asian winter monsoon variability. *J Clim* 27:5433–5450
- Chen SF, Wu RG, Chen W et al (2020) Weakened impact of autumn Arctic sea ice concentration change on the subsequent winter Siberian High variation around the late 1990s. *Int J Climatol* 41:2700–2717
- Ding QH (2021) Internal atmospheric processes contributing to Arctic summer rapid warming and ice melting in recent 20 years. *Trans Atmos Sci* 44:39–49 (in Chinese)
- Duan AM, Wu GX (2008) Weakening trend in the atmospheric heat source over the Tibetan Plateau during recent decades. Part I: Observations. *J Clim* 21:3149–3155
- Dunn RJH, Alexander LV, Donat MG et al (2020) Development of an updated global land in situ-based data set of temperature and precipitation extremes: HadEX3. *J Geophys Res Atmos* 125:e2019JD032263
- Gao YQ, Sun JQ, Li F et al (2015) Arctic sea ice and Eurasian climate: a review. *Adv Atmos Sci* 32:92–114
- Gu S, Zhang Y, Wu QG et al (2018) The linkage between Arctic sea ice and mid latitude weather: in the perspective of energy. *J Geophys Res Atmos* 123:11536–11550
- Hersbach H, Bell B, Berrisford P et al (2020) The ERA5 global reanalysis. *Q J R Meteorol Soc* 146:1999–2049
- Honda M, Inoue J, Yamane S (2009) Influence of low Arctic sea-ice minima on anomalously cold Eurasian winters. *Geophys Res Lett* 36:262–275
- Hopsch S, Cohen J, Dethloff K (2012) Analysis of a link between fall Arctic sea ice concentration and atmospheric patterns in the following winter. *Tellus Ser A Dyn Meteorol Oceanogr* 64:389–400
- Hu ZZ, Huang BH (2006) On the significance of the relationship between the North Atlantic Oscillation in early winter and Atlantic sea surface temperature anomalies. *J Geophys Res Atmos*. <https://doi.org/10.1029/2005JD006339>
- Hu ZZ, Wu ZH (2004) The intensification and shift of the annual North Atlantic Oscillation in a global warming scenario simulation. *Tellus Ser A Dyn Meteorol Oceanogr* 56(2):112–124
- Hu ZZ, Kuzmina SI, Bengtsson L et al (2004) Sea-ice change and its connection with climate change in the Arctic in CMIP2 simulations. *J Geophys Res Earth Surf*. <https://doi.org/10.1029/2003JD004454>
- Inoue J, Hori ME, Takaya K (2012) The role of Barents sea ice in the wintertime cyclone track and emergence of a warm-Arctic cold-Siberian anomaly. *J Clim* 25:2561–2568
- Jaiser R, Dethloff K, Hondorf D et al (2012) Impact of sea ice cover changes on the northern hemisphere atmospheric winter circulation. *Tellus Ser A Dyn Meteorol Oceanogr* 64:53–66
- Jiao Y, You QL, Lin HB et al (2017) Relationship of Arctic sea ice coverage anomalies in summer-autumn and extreme cold days over the Tibetan Plateau in autumn-winter and the mechanism. *Clim Environ Res* 22:435–445 (in Chinese)

- Karl TR, Nicholls N, Ghazi A (1999) CLIVAR/GCOS/WMO workshop on indices and indicators for climate extremes workshop summary. *Clim Change* 42:3–7
- Kim B-M, Son S-W, Min S-K et al (2014) Weakening of the stratospheric polar vortex by Arctic sea-ice loss. *Nat Commun* 5:7–8
- Koenigk T, Barring L, Matei D et al (2020) On the contribution of internal climate variability to European future climate trends. *Tellus Ser A Dyn Meteorol Oceanogr* 72:1–17
- Li QQ, Yang S, Kousky VE et al (2005) Features of cross-Pacific climate shown in the variability of China and US precipitation. *Int J Climatol* 25:1675–1696
- Li F, Wan X, Wang HJ et al (2020) Arctic sea-ice loss intensifies aerosol transport to the Tibetan Plateau. *Nat Clim Chang* 10:1037–1044
- Li HX, Sun B, Zhou BT et al (2021) Effect of march Barents sea ice on august temperature dipole pattern in eastern china and its mechanism. *Trans Atmos Sci* 44:89–103 (in Chinese)
- Liu G, Wu RG, Zhang YZ et al (2014) The summer snow cover anomaly over the Tibetan Plateau and its association with simultaneous precipitation over the Mei-yu-Baiu region. *Adv Atmos Sci* 31:755–764
- Lu LH, Bian LG, Zhang ZQ (2011) Climate change and its impacts in the polar and Tibetan Plateau. *Chin J Polar Res* 23:82–89 (in Chinese)
- Ma SM, Zhu CW (2019) Extreme cold wave over East Asia in January 2016: a possible response to the larger internal atmospheric variability induced by Arctic warming. *J Clim* 32:1203–1216
- Ma SM, Zhu CW (2020) Opposing trends of winter cold extremes over Eastern Eurasia and North America under recent Arctic warming. *Adv Atmos Sci* 37:1417–1434
- Outten SD, Esau I (2012) A link between Arctic sea ice and recent cooling trends over Eurasia. *Clim Change* 110:1069–1075
- Overland JE, Wang MY, Wood KR et al (2012) Recent Bering Sea warm and cold events in a 95-year context. *Deep Sea Res Part II* 65–70:6–13
- Peings Y, Magnusdottir G (2014) Response of the wintertime northern hemisphere atmospheric circulation to current and projected Arctic sea ice decline: a numerical study with CAM5. *J Clim* 27:244–264
- Peterson TC (2005) Climate change indices. *World Meteorol Organ Bull* 54(2):83–86
- Rayner NA, Parker DE, Horton EB et al (2003) Global analyses of sea surface temperature, sea ice, and night marine air temperature since the late nineteenth century. *J Geophys Res Atmos*. <https://doi.org/10.1029/2002JD002670>
- Ren CY, Duan MK, Zhi XF (2017) Analysis of extreme temperature characteristics in winter and summer under different climate background in China. *Trans Atmos Sci* 40:803–813 (in Chinese)
- Ren Q, Jiang X, Zhang Y, Li Z, Yang S (2021) Effects of suppressed transient eddies by the Tibetan Plateau on East Asian summer monsoon. *J Clim*. <https://doi.org/10.1175/JCLI-D-20-0646.1>
- Suolang TJ, Shi N, Wang YC et al (2020) Interdecadal variation characteristics of extreme low temperature index in winter in China. *Chin J Atmos Sci* 44(5):1125–1140 (in Chinese)
- Takaya K, Nakamura H (2001) A formulation of a phase-independent wave activity flux for stationary and migratory quasi geostrophic eddies on a zonally varying basic flow. *J Atmos Sci* 58:608–627
- Wallace JM, Lim G-H, Blackmon ML (1988) Relationship between cyclone tracks, anticyclone tracks and baroclinic waveguides. *J Atmos Sci* 45:439–462
- Wu BY (2018) Research progress on the influence of Arctic sea ice melting on winter weather and climate in East Asia. *Adv Earth Sci* 42:786–805 (in Chinese)
- Wu BY, Huang RH, Gao DY (1999) Effects of variation of winter sea ice area in Kara and Barents seas on East Asia winter monsoon. *J Meteorol Res* 13:141–153
- Wu SH, Yin YH, Zheng D et al (2005) Climate change trend of Tibet Plateau in recent 30 years. *Acta Geogr Sinica* 60:3–11 (in Chinese)
- Wu BY, Su JZ, Zhang RH (2011) Effects of autumn-winter Arctic sea ice on winter Siberian High. *Chin Sci Bull* 56:3220–3228
- Wu BY, Handorf D, Dethloff K et al (2013) Winter weather patterns over northern Eurasia and Arctic sea ice loss. *Mon Weather Rev* 141:3786–3800
- Wu BY, Su JZ, D'Arrigo R (2015) Patterns of Asian winter climate variability and links to Arctic sea ice. *J Clim* 28:6841–6858
- Wu BY, Yang K, Francis JA (2017) A cold event in Asia during January–February 2012 and its possible association with Arctic sea ice loss. *J Clim* 30:7971–7990
- Wu LQ, Li QQ, Ding YH et al (2018) Preliminary assessment on the hindcast skill of the arctic oscillation with decadal experiment by the BCC\_CSM1.1 climate model. *Adv Clim Change Res* 9(4):209–217
- Wu FM, Li WK, Li W (2019a) Research progress on the cause of Arctic amplification effect. *Adv Earth Sci* 34:232–242 (in Chinese)
- Wu TW, Lu YX, Fang YJ et al (2019b) The Beijing Climate Center climate system model (BCC-CSM): main progress from CMIP5 to CMIP6. *Geosci Mod Dev* 12:1573–1600
- Yang S, Lau K-M, Kim K-M (2002) Variations of the east Asian jet stream and Asian–Pacific–American winter climate anomalies. *J Clim* 15:306–325
- Yang DD, Zhang LJ, Zhou S et al (2020) Variation of winter extreme cold events in northern hemisphere and its relationship with autumn sea ice. *Plateau Meteorol* 39:102–109 (in Chinese)
- Zahn M, Von SH (2010) Decreased frequency of North Atlantic polar lows associated with future climate warming. *Nature* 467:309–312
- Zhang Y, Zou T, Xue Y (2019) An Arctic-Tibetan connection on subseasonal to seasonal time scale. *Geophys Res Lett* 46(10):2790–2799
- Zhao JP, Shi JX, Wang ZM et al (2015) Arctic amplification mechanism and global climate effect caused by Arctic sea ice decline. *Adv Earth Sci* 30:985–995 (in Chinese)
- Zhou YK (2019) Characterizing the spatio-temporal dynamics and variability in climate extremes over the Tibetan Plateau during 1960–2012. *J Resour Ecol* 10:397–414
- Zhu CW, Chen LX, Yamazaki N (1999) The interdecadal variation characteristics of Arctic sea ice cover-ENSO-East Asian monsoon and their interrelationship at quasi-four years time scale. *Adv Atmos Sci* 16:641–652

**Publisher's Note** Springer Nature remains neutral with regard to jurisdictional claims in published maps and institutional affiliations.